

Supplementary Information

Highly selective CO₂/CH₄ gas uptake by a halogen-decorated borazine-linked polymer

Thomas E. Reich, S. Behera, Karl T. Jackson, Puru Jena, and Hani M. El-Kaderi*

Department of Chemistry, Department of Physics, Virginia Commonwealth University, Richmond, Virginia 23284-2006

Table of Contents

Section S1	<i>FT-IR Spectroscopy</i>	S2
Section S2	<i>Solid-State ¹¹B and ¹³C Magic Angle Spinning (MAS) Nuclear Magnetic Resonance</i>	S5
Section S3	<i>Scanning Electron Microscopy (SEM) Imaging</i>	S7
Section S4	<i>Thermogravimetric Analysis (TGA)</i>	S8
Section S5	<i>Low Pressure (0 – 1.0 bar) Nitrogen and Hydrogen Gas Adsorption Measurements</i>	S9
Section S6	<i>Computational Methodology</i>	S21
Section S7	<i>Selectivity and the Ideal Adsorbed Solution Theory (IAST)</i>	S27

Section S1: *FT-IR Spectroscopy for BLP-10(Cl) and the Starting Materials*

FT-IR spectra were obtained as KBr pellets using a Nicolet Nexus 670 FT-IR spectrometer. FT-IR spectra were obtained to verify the production of the intended products coupled with the loss of starting material. The fading of certain peaks like amine stretching combined with the appearance of borazine-characteristic peaks supports the production of the intended products.

Figure S1: FT-IR spectrum of benzidine.

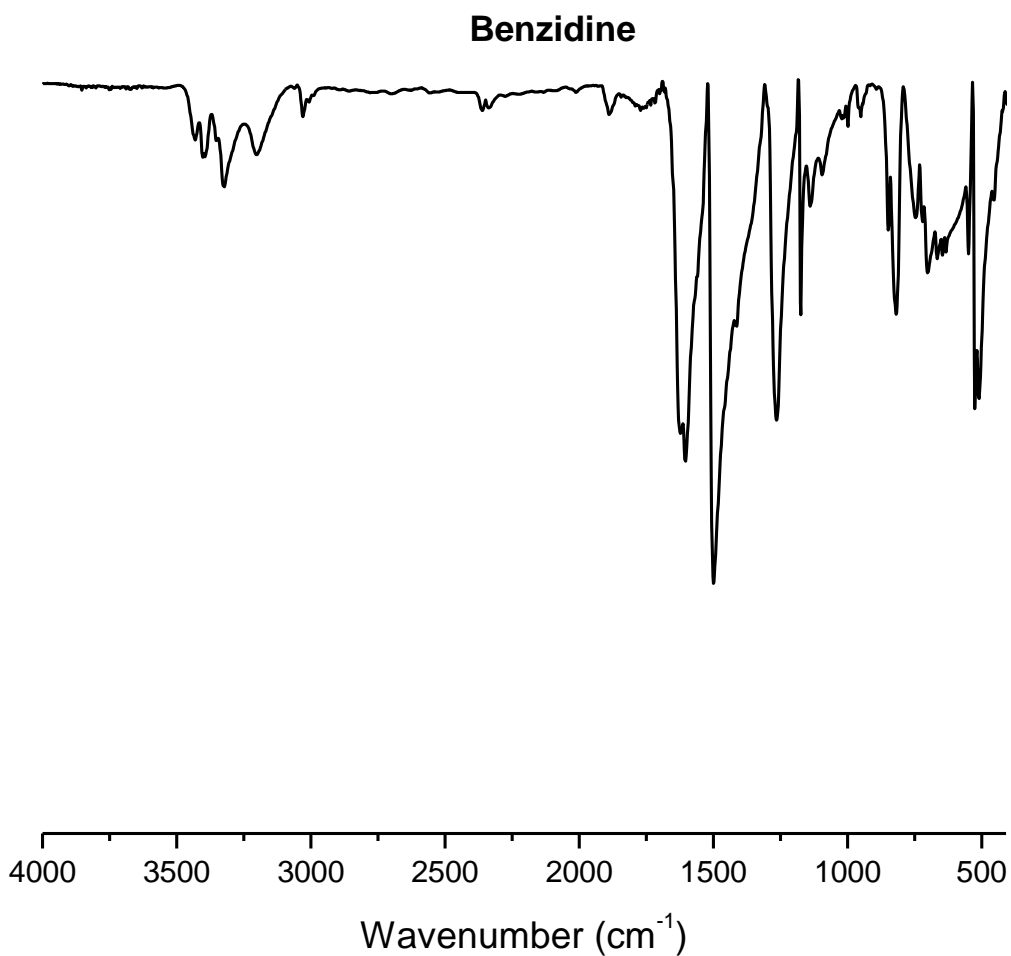


Figure S2: FT-IR spectrum of BLP-10(Cl).

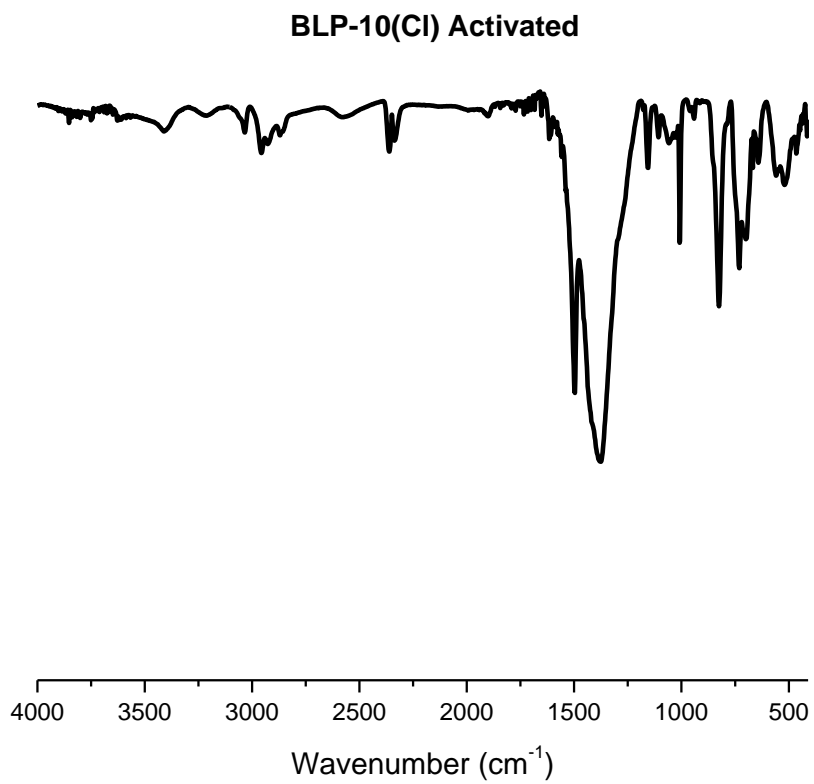
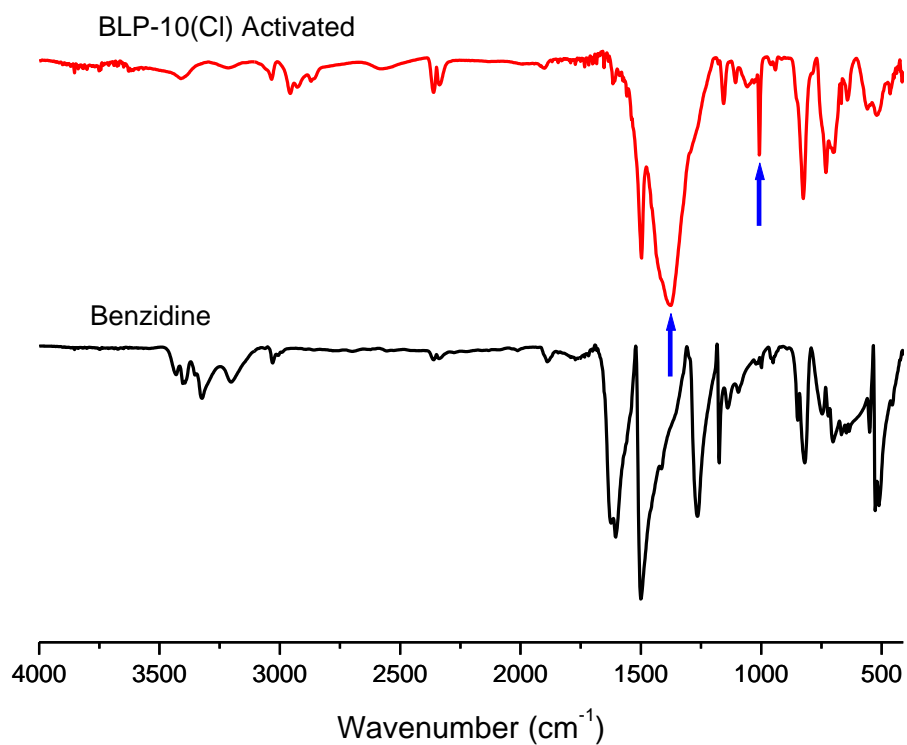


Figure S3: IR spectra of BLP-10(Cl) with its starting material, benzidine. The largely diminished amine stretching and bending bands indicate the consumption of benzidine. The peaks around 1400 and 1000 cm^{-1} is consistent with borazine ring formation.¹



Section S2: *Solid-State ^{11}B and ^{13}C Magic Angle Spinning (MAS) Nuclear Magnetic*

^{11}B MAS NMR data were collected with a 45 degree ^{11}B pulse length and a recycle delay of two seconds. High-power H-1 decoupling was employed during acquisition only. Samples were spun at the magic angle at about 7 kHz. Chemical shifts are referenced to external neat boron trifluoroetherate. Solid-state NMR spectra were recorded at ambient temperature on a 360-1 instrument by Spectral Data Services, Inc., Champaign, IL. *Asterisks represent spinning side bands.*

Figure S4: Solid-state ^{11}B NMR spectrum of BLP-10(Cl).

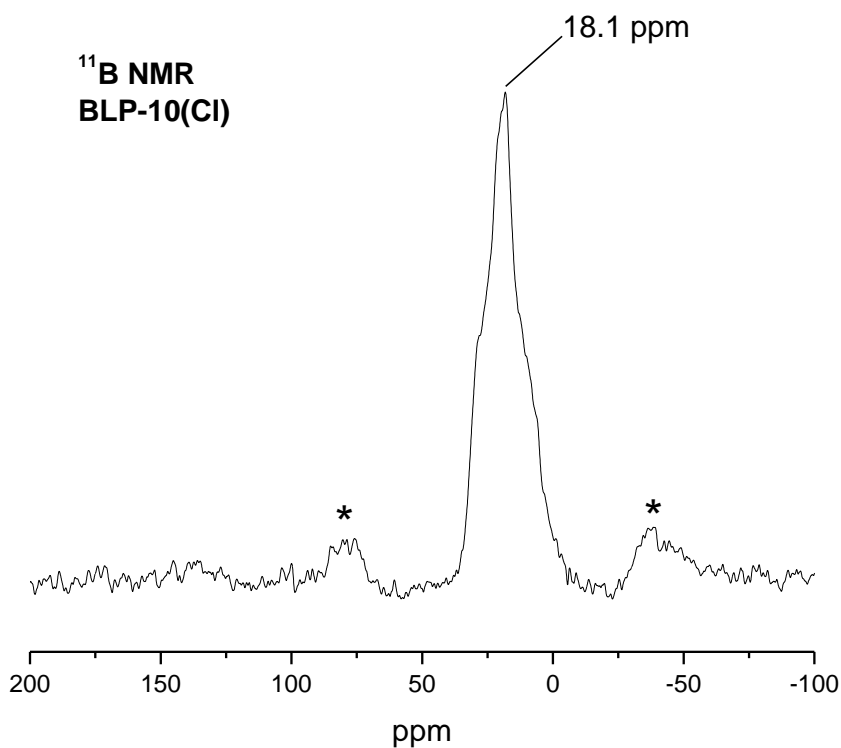


Figure S5: Solid-State ^{13}C NMR Spectrum of BLP-10(Cl). All of the expected peaks from the starting material are present in BLP-10(Cl), which indicates that the backbone of the aryl amine building block survived the reaction. Some of the carbon signals are too close in chemical shift to be resolved. Peak assignments are shown in Table S1.

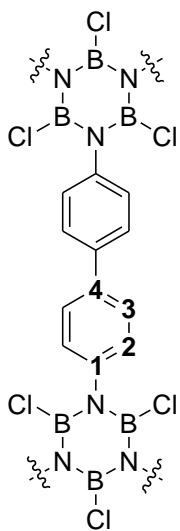
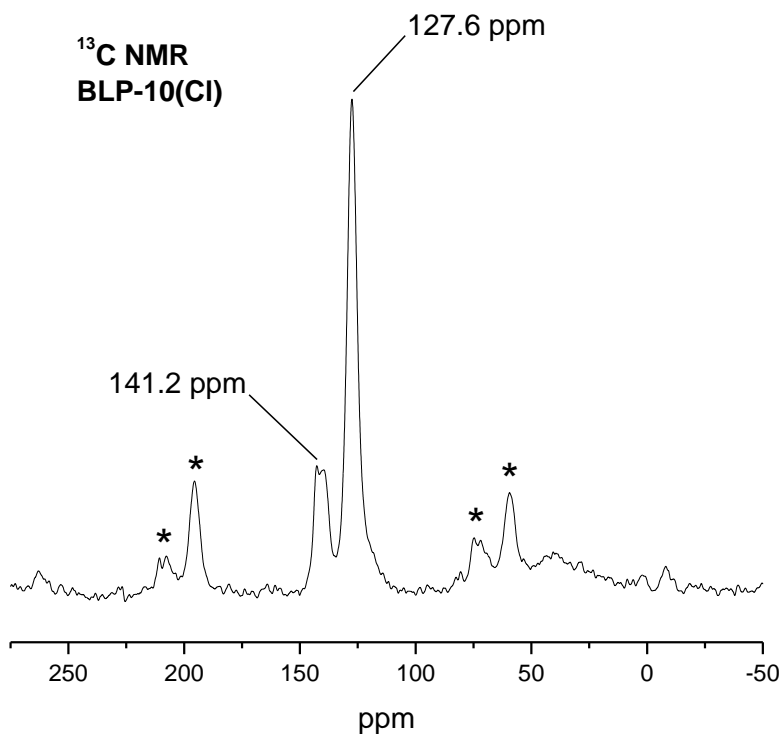


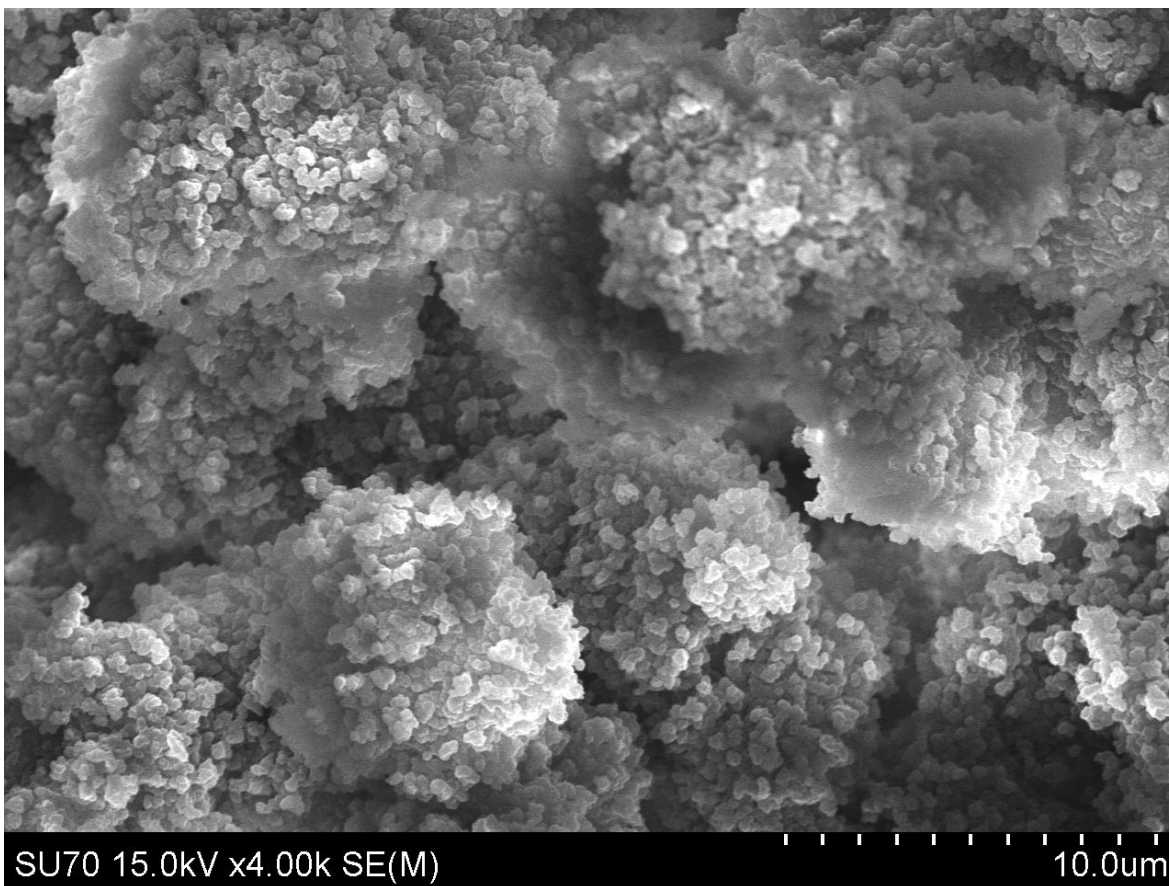
Table S1. ^{13}C NMR peak assignments for BLP-10(Cl).

Carbon	Chemical Shift (ppm)
1	141.2
2	127.6
3	127.6
4	127.6

Section S3: Scanning Electron Microscopy (SEM) Imaging

To assess the purity of the products, SEM imaging was used to detect the level of morphological diversity. BLP-10(Cl) exists as irregular particles of about 100-300 nm in size. Samples were prepared by dispersing the material onto a sticky carbon surface attached to a flat aluminum sample holder. The samples were then gold coated using an EMS (Electron Microscopy Sciences) 550x Sputter Coater at 1×10^{-1} mbar of pressure in a nitrogen atmosphere for 120 seconds while maintaining 20 mA of current. Samples were analyzed on a Zeiss EVO XVP Scanning Electron Microscope using the SEI detector with accelerating voltages ranging from 10 kV to 20 kV.

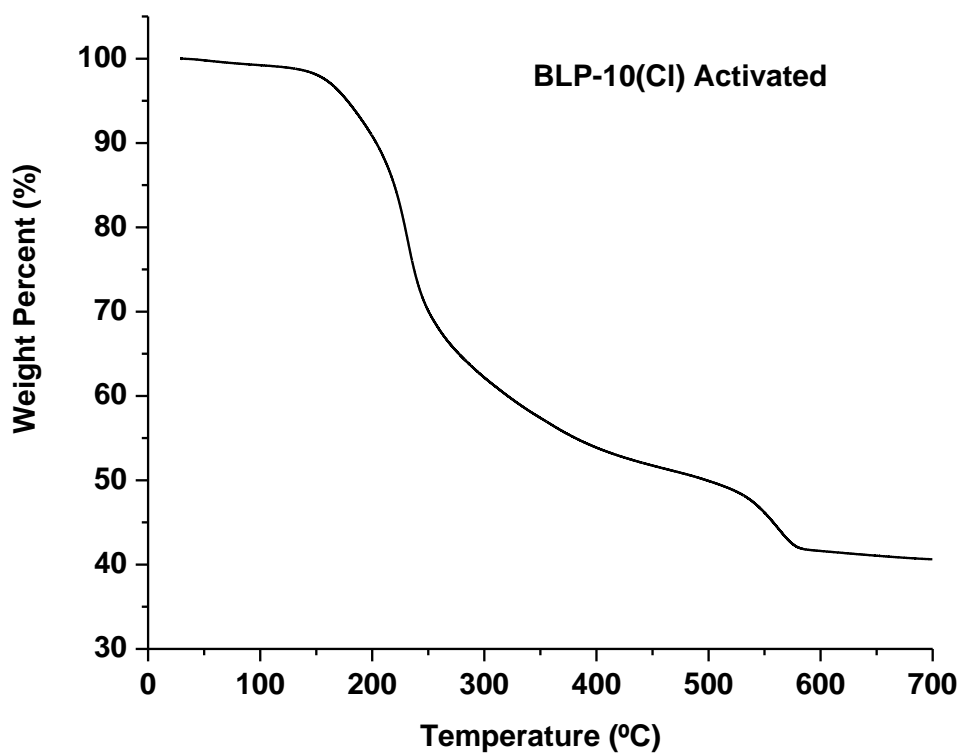
Figure S6: SEM image of as-prepared BLP-10(Cl).



Section S4: Thermogravimetric Analysis (TGA)

Thermogravimetric analysis was obtained using a TA Instruments TGA Q5000 analyzer with 50 μL platinum pans to assess the thermal stability of each borazine-linked polymer. Experiments were run at a ramp rate of 5 K/minute under a nitrogen atmosphere.

Figure S7: TGA for an activated sample of BLP-10(Cl).



Section S5: *Low Pressure (0 – 1.0 bar) Nitrogen, Hydrogen, Carbon Dioxide, and Methane Gas Adsorption Measurements*

Nitrogen sorption experiments were run to determine surface area and pore size distribution. Nitrogen experiments were run using a Quantachrome Autosorb 1-C analyzer at 77 K. Further nitrogen experiments for ideal adsorbed solution theory were run at 298 K.

Hydrogen, carbon dioxide, and methane sorption experiments were run on the same Quantachrome Autosorb 1-C analyzer. Hydrogen experiments were run at 77 K and 87 K, and carbon dioxide and methane experiments were run at 273 K and 298 K. Isothermic heats of adsorption for each gas were calculated using the virial-type expansion.²

Pore Size Distribution (PSD) was calculated using Non-Local Density Functional Theory (NLDFT) on the adsorption branch with a cylindrical pore model on the nitrogen sorption data (77 K) and carbon dioxide sorption data (273 K) in accordance with previously reported literature.³

Figure S8: Nitrogen isotherm for BLP-10(Cl) measured at 77K.

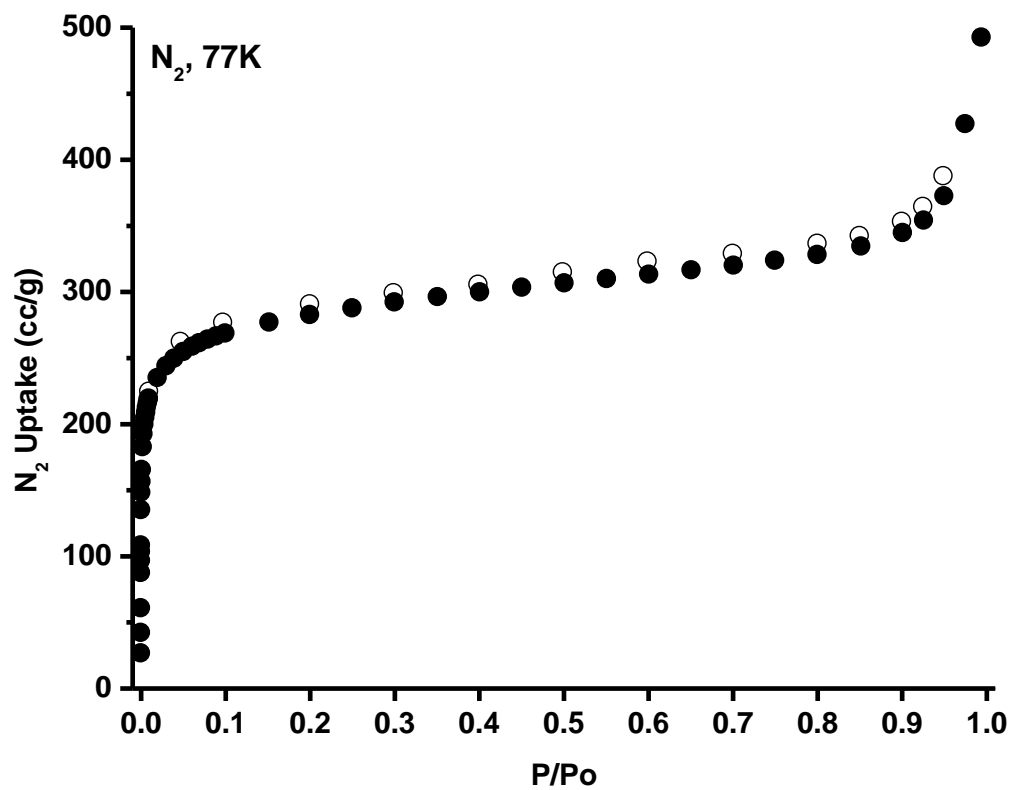


Figure S9: Pore Size Distribution (PSD) for BLP-10(Cl) using the NLDFT model.

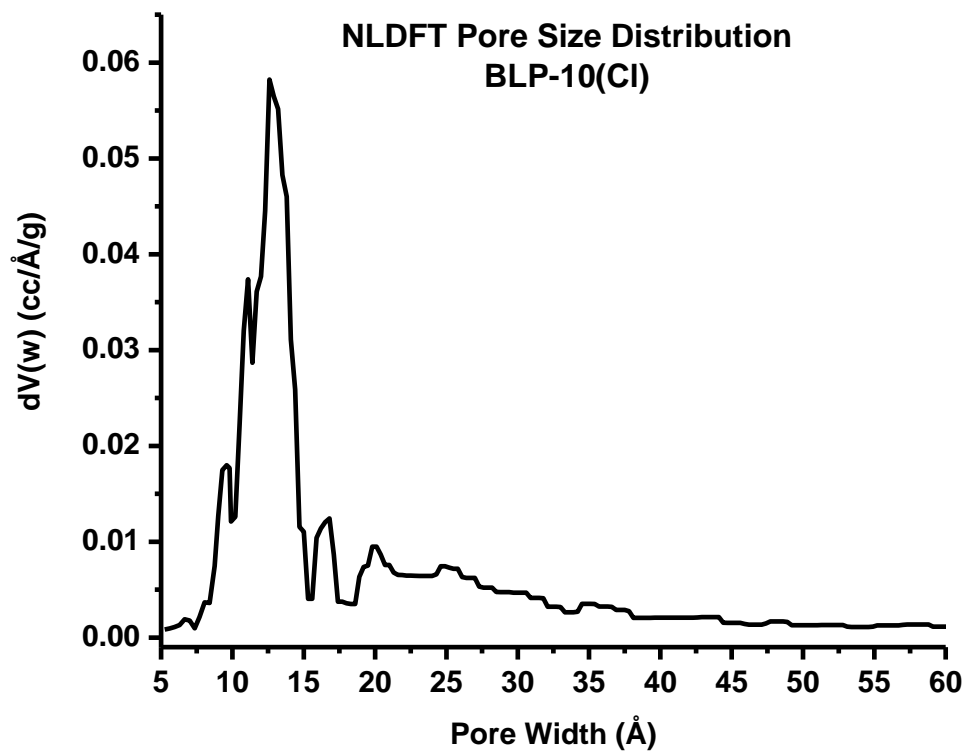


Figure S10: NLDFT calculated isotherm for BLP-10(Cl) overlaid with the experimental nitrogen isotherm. A fitting error less than 1% indicates validity of the model.

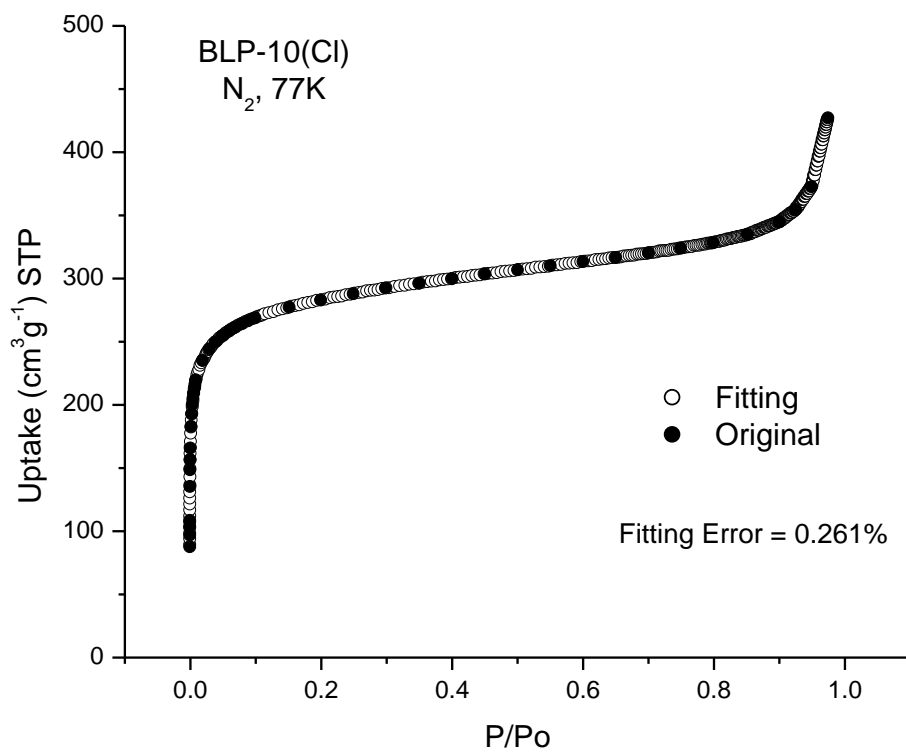


Figure S11: Langmuir plot for BLP-10(Cl) calculated from the nitrogen adsorption in the range 0.05-0.30 P/P_0 .

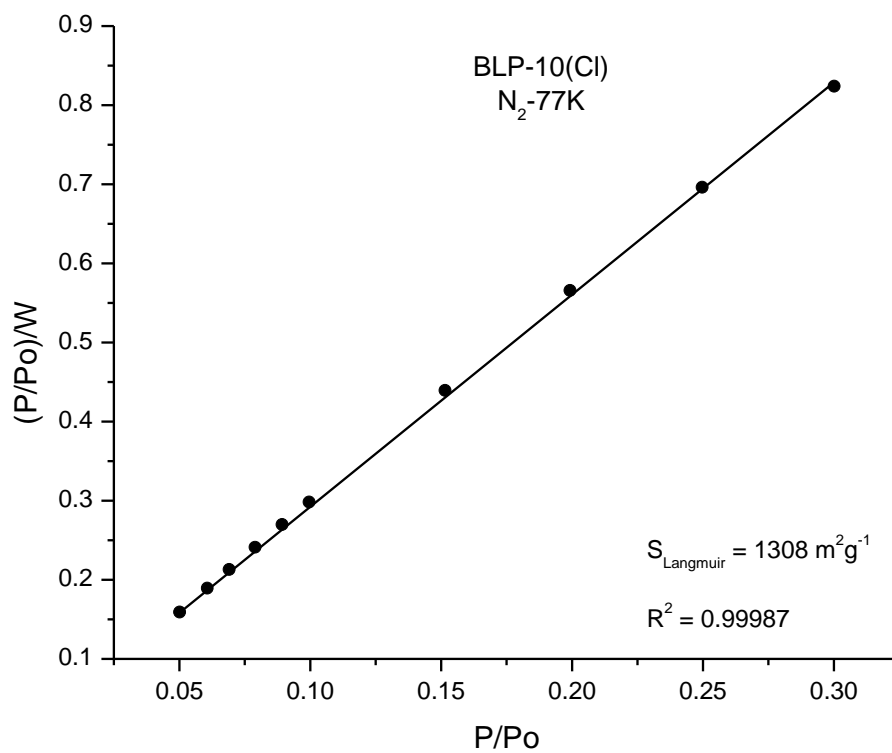


Figure S12: Multipoint BET plot for BLP-10(Cl) calculated from the nitrogen adsorption in the range 0.02-0.20 P/P₀.

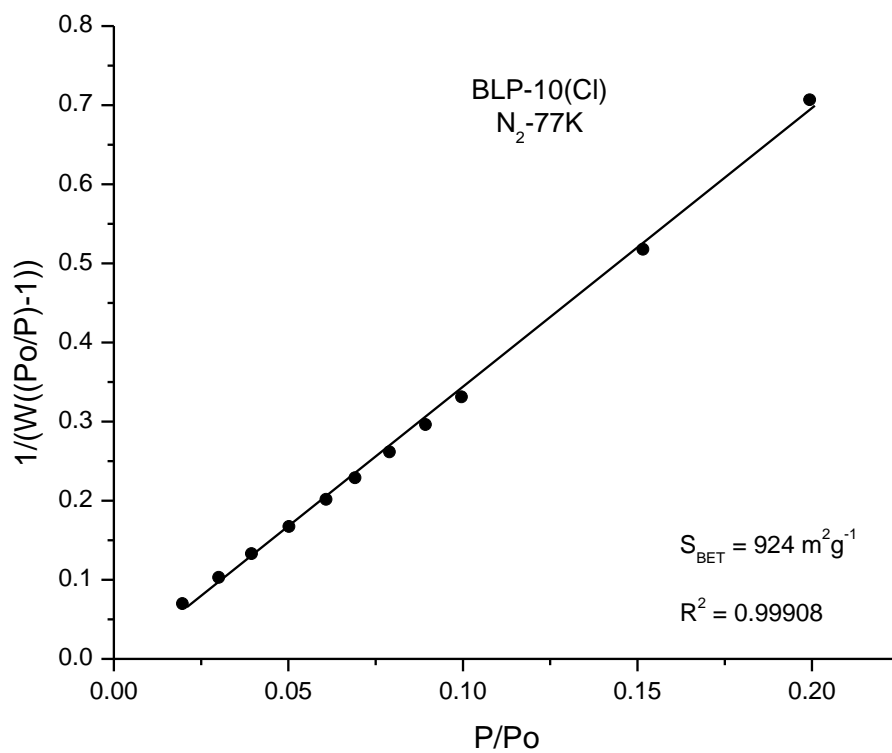


Figure S13: Hydrogen isotherm for BLP-10(Cl) at 77 and 87 K. The virial coefficients are shown for the fitting (solid lines). R^2 values for the 77 K and 87 K curves are 0.99999 and 0.99999, respectively.

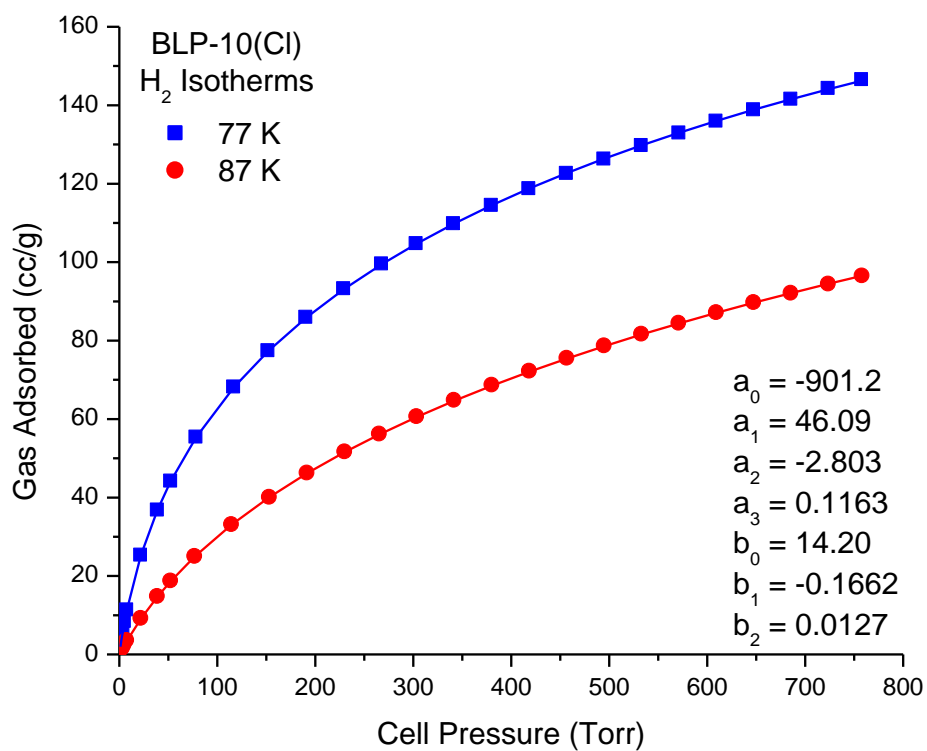


Figure S14: Carbon dioxide isotherm for BLP-10(Cl) at 273 and 298 K. The virial coefficients are shown for the fitting (solid lines). R^2 values for the 273 K and 298 K curves are 0.99998 and 0.99988, respectively.

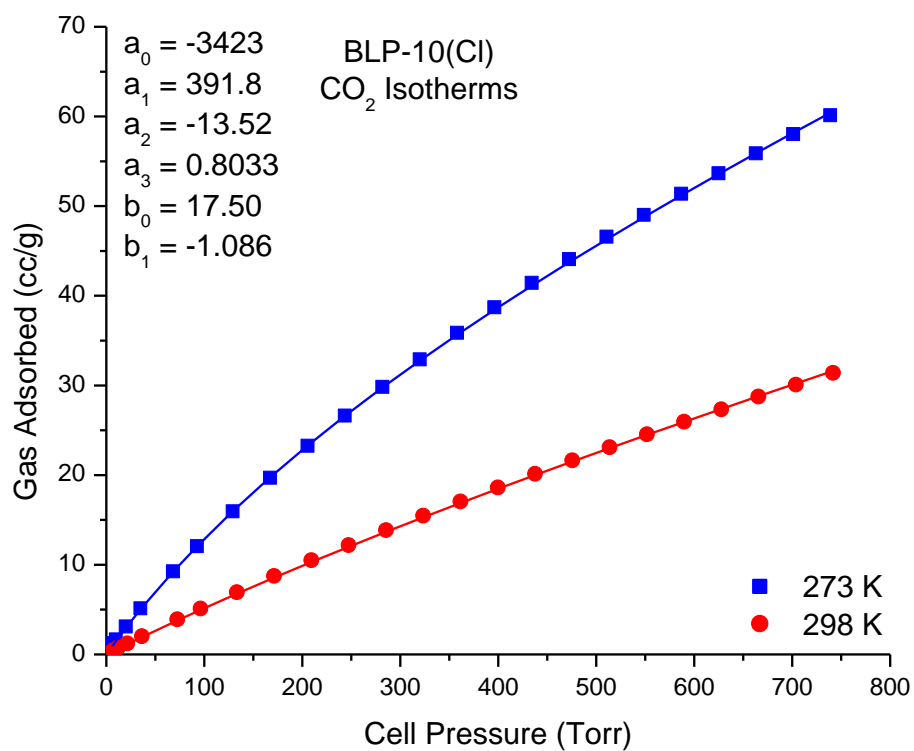


Figure S15: Methane isotherm for BLP-10(Cl) at 273 and 298 K. The virial coefficients are shown for the fitting (solid lines). R^2 values for the 273 K and 298 K curves are 0.99974 and 0.99921, respectively.

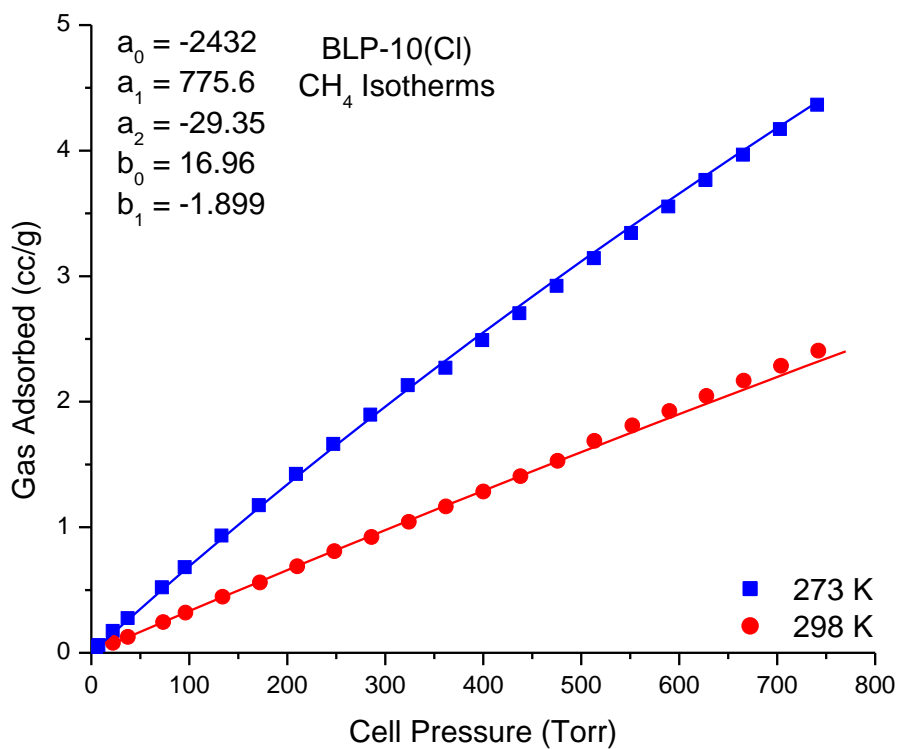


Figure S16: Isothermic heat of adsorption, Q_{st} , for hydrogen.

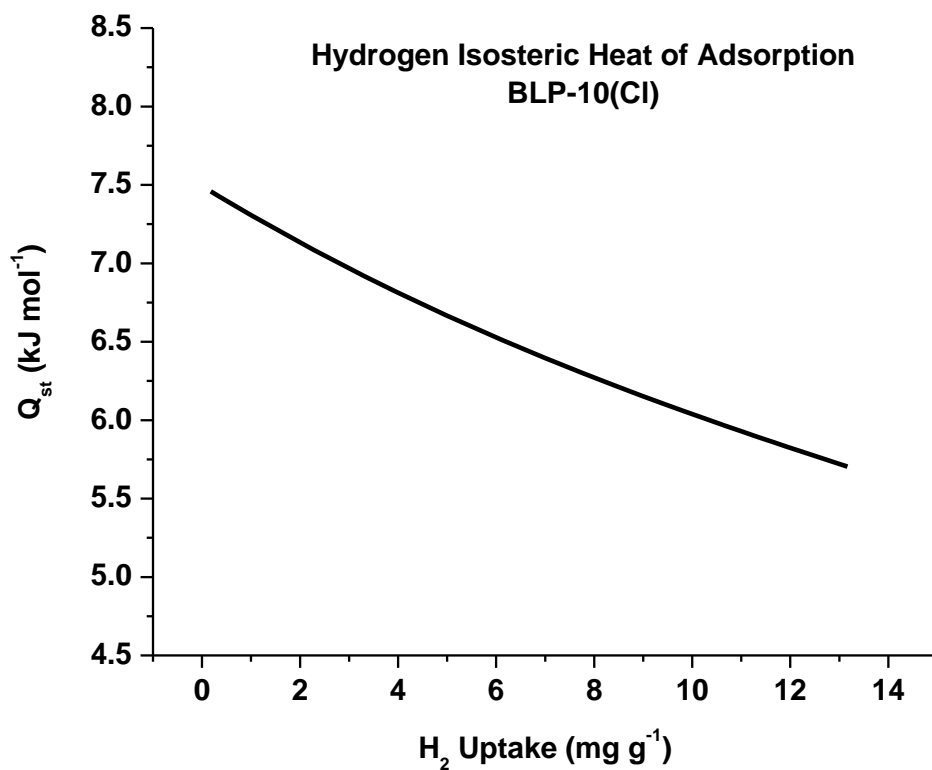


Figure S17: Isosteric heat of adsorption, Q_{st} , for carbon dioxide.

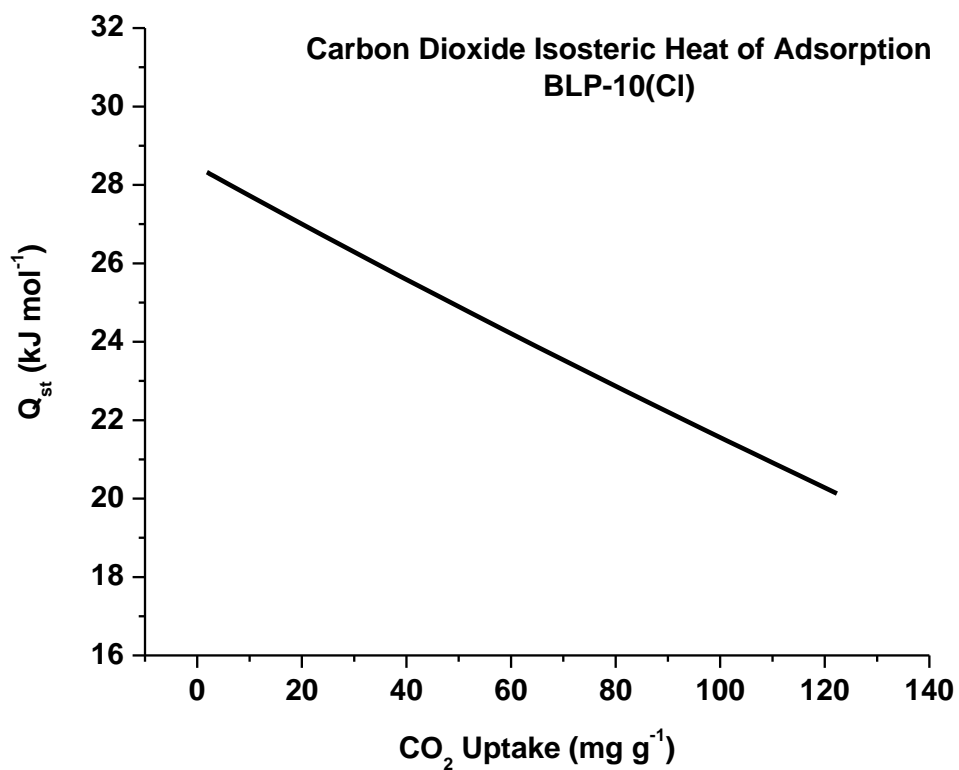
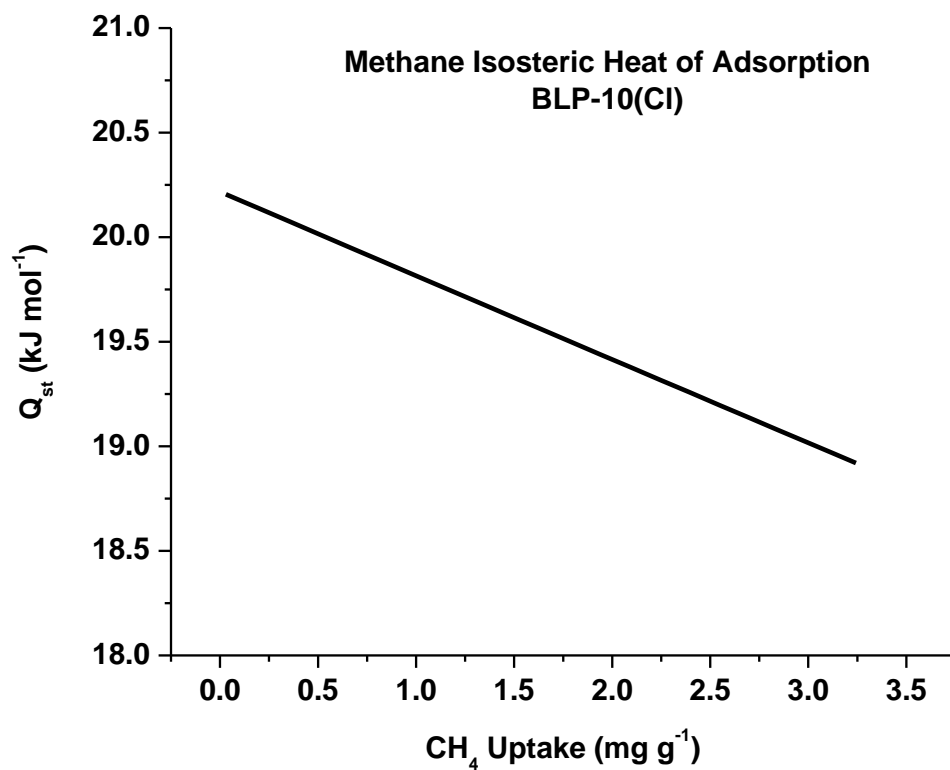


Figure S18: Isostatic heat of adsorption, Q_{st} , for methane.



Section S6: Computational Methodology

To ease the computational load, the polymeric system was simplified to a monomeric chlorinated borazine bound to three phenyl rings through the nitrogen atoms. The binding affinities, E_b of H_2 , CO_2 and CH_4 molecules attached to chlorinated borazines (CB) were calculated by determining the equilibrium geometries and corresponding total energies of these complexes. We define E_b as,

$$E_b = -\{E[(CB).x] - E[CB] - E[x]\};$$

where x denotes H_2 , CO_2 or CH_4 molecule; $E[(CB).x]$ is the total energy of the chlorinated borazine interacting with H_2 , CO_2 or CH_4 ; and $E[CB]$ and $E[x]$ are, respectively, the total energies of the CB and the x molecule. All calculations were done using density functional theory (DFT) with different forms for exchange-correlation potential. These include the Becke's three parameter hybrid functional for exchange and Lee-Yang-Parr functional for correlation (B3LYP),⁴ the local density approximation (LDA) for exchange-correlation potential prescribed by Vosko-Wilk-Nusair (SVWN)⁵ and the functional of Zhao and Truhlar (M06)⁶ that includes corrections for long range dispersive forces. We note that since the interaction of H_2 , CO_2 or CH_4 with the CB substrate is expected to be weak, it is necessary to go beyond the generalized gradient functionals that do not include van der Waal's terms and hence underestimate binding affinities. While LDA also does not include long range dispersive forces, it is known to over-bind. Thus, it is possible that due to cancellation of errors LDA may yield binding affinities that are closer to experiment than the GGA functionals. This is found indeed to be the case. We have used *Gaussian 09* package⁷ and 6-311+G*^{8,9} basis sets for all our computations. The convergence in the total energy and force were set at 1×10^{-6} eV and

1×10^{-2} eV/Å, respectively. The output symmetries were kept at a tolerance of 0.1 using Gaussview.

Several initial geometries were taken where the molecules were allowed to approach different sites of CB including the top of the borazine ring, the bridge sites as well as on top of B and N atoms. The molecules were further allowed to align perpendicular or parallel to the ring surface. The geometries were first optimized without symmetry constraint at the B3LYP level of theory. These geometries were used again as starting configurations with other functionals such as M06 and SVWN and re-optimized. All optimization are followed by frequency calculations to confirm that the structures represent genuine minima in the potential energy surface. The atomic charges have been evaluated by applying the Natural Bonding Orbital method (NBO).¹⁰ The theoretically calculated binding affinities (E_b) using different methods are compared with the experimental results and are shown in the Table S2. Since the B3LYP results are unphysical for H₂ and CH₄, we did not repeat the calculations for CO₂.

Table S2: Comparison of calculated binding affinity of CO₂, H₂ and CH₄ to CB (chlorinated borazine) with experimental values:

Clusters	Expt (kJ/mol)	B3LYP/6- 311+G* (kJ/mol)	M06/6- 311+G* (kJ/mol)	SVWN/6- 311+G* (kJ/mol)
CB - H ₂	7.46	-2.33	9.05	10.39
CB- CO ₂	28.28	-	15.46	25.95
CB -CH ₄	20.2	-0.22	20.22	20.30

Figure S19: Optimized geometries of (a) H₂, (b) CO₂ and (c) CH₄ adsorbed on chlorinated borazine calculated at M06/6-311+G* level of theory. The bond lengths are in Å. Front and side views are given (left and right panel, respectively). The blue, pink, green, grey, white, and red colors stand for N, B, Cl, C, H, and O atoms, respectively.

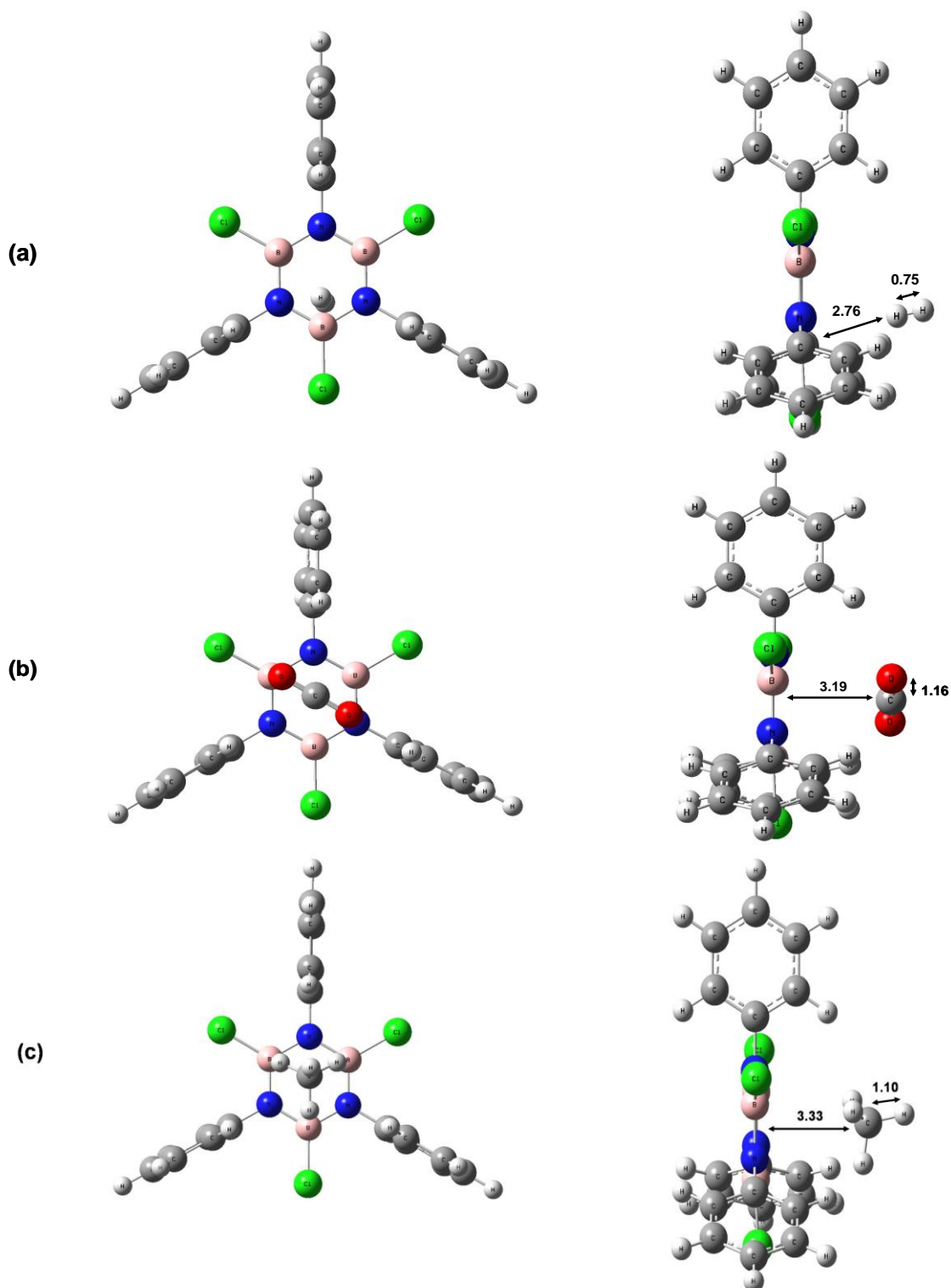


Figure S20: Optimized geometries of (a) H₂, (b) CO₂ and (c) CH₄ adsorbed on chlorinated borazine calculated at SVWN/6-311+G* level of theory. The bond lengths are in Å. Front and side views are given on the left and right panel, respectively. The blue, pink, green, grey, white, and red colors stand for N, B, Cl, C, H, and O atoms, respectively.

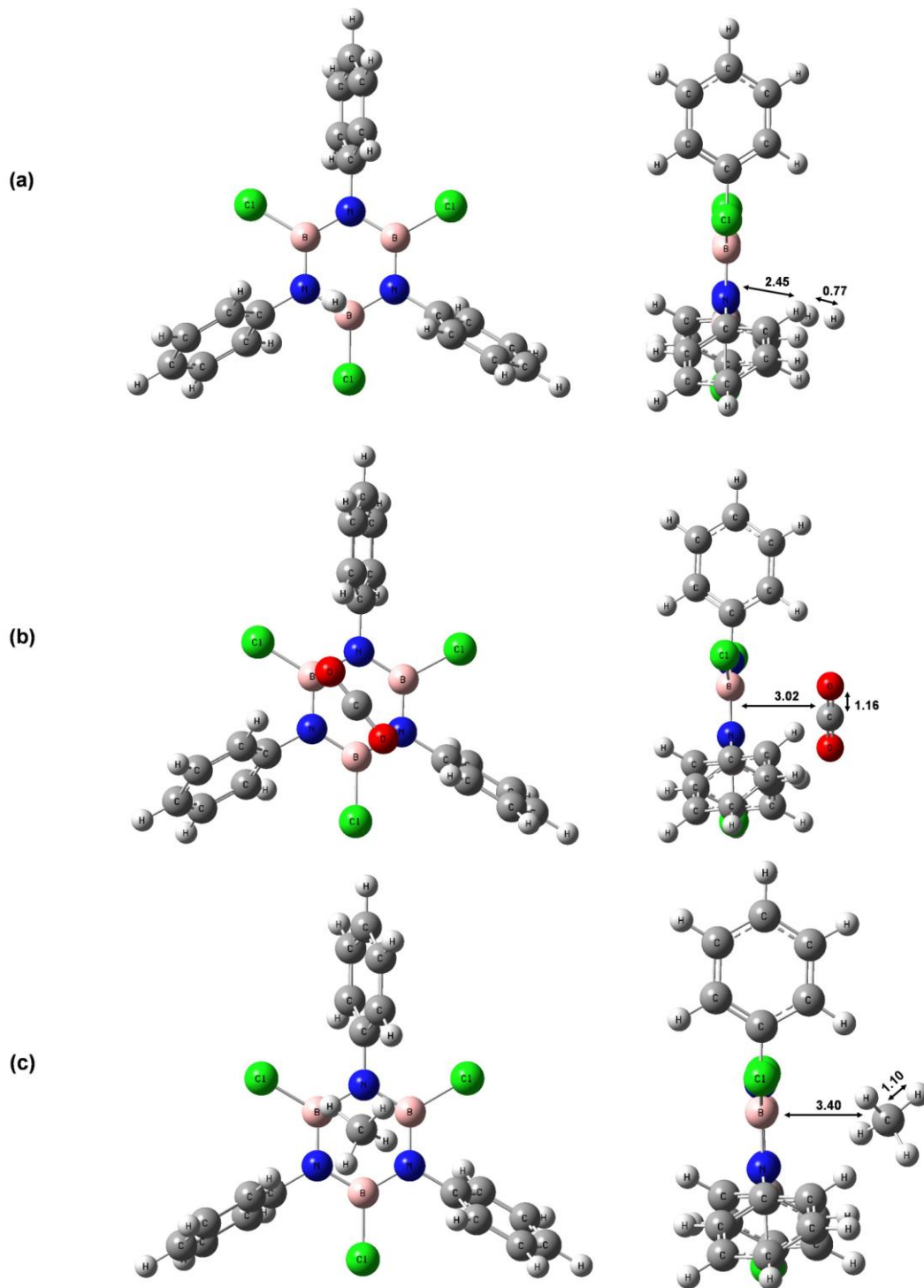
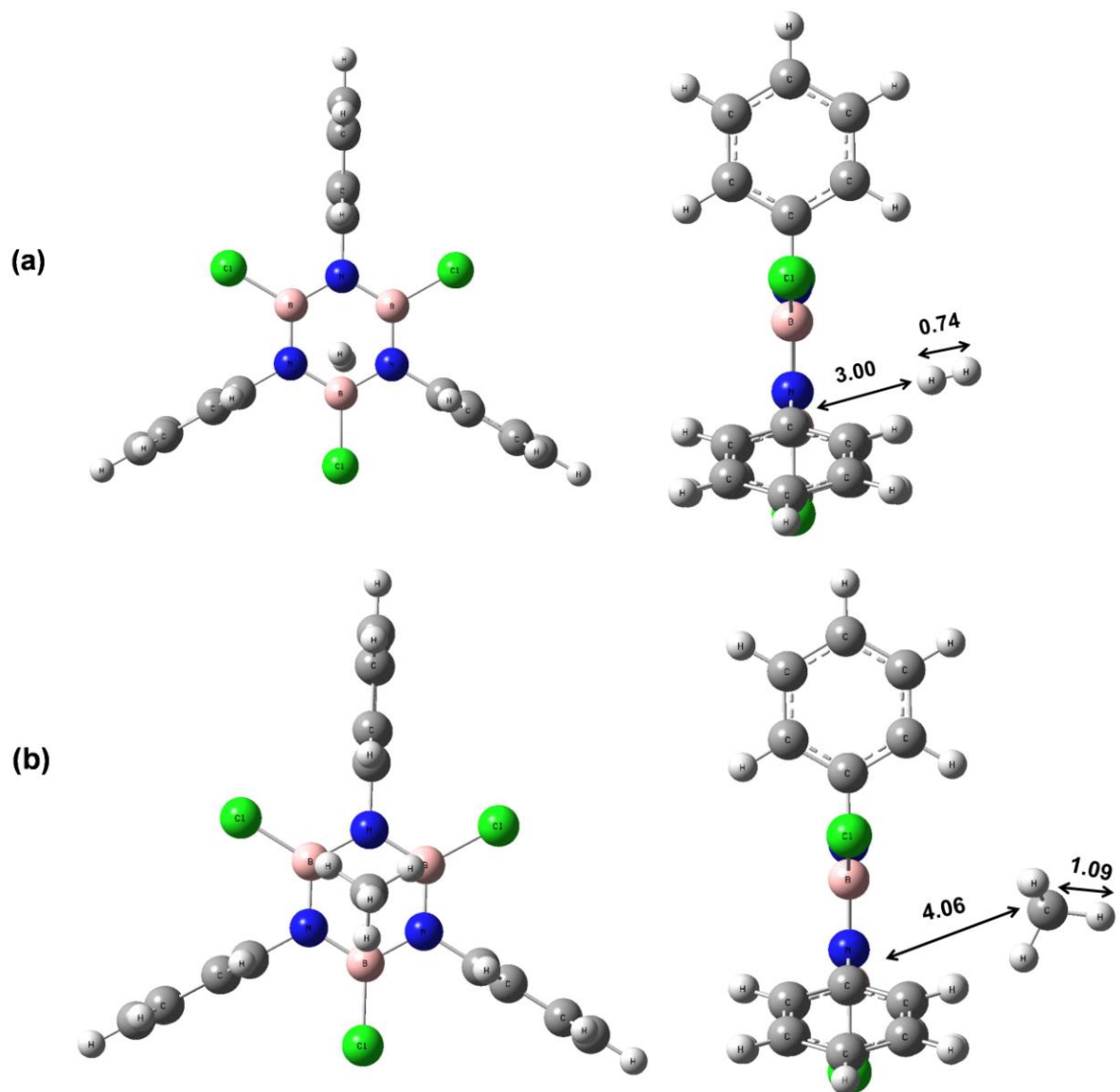


Figure S21: Optimized geometries of (a) H₂, (b) CH₄ adsorbed on chlorinated borazine calculated at B3LYP/6-311+G* level of theory. The bond lengths are in Å. Front and side views are given on the left and right panel, respectively. The blue, pink, green, grey, white, and red colors stand for N, B, Cl, C, H, and O atoms, respectively.



Section S7: *Selectivity and the Ideal Adsorbed Solution Theory (IAST)*

Ideal adsorbed solution theory calculations were performed as has been previously reported.^{11,12} According to Myers and Prausnitz,¹ the ideal adsorbed solution theory can be reduced to the mathematical integration:

$$\int_{t=0}^{\frac{Py_1}{x_1}} F_1(t) d \ln t = \int_{t=0}^{\frac{Py_2}{x_2}} F_2(t) d \ln t$$

In this equation, P is the total pressure, y_i is the bulk phase molar ratio of gas i, x_i is the adsorbed phase molar ratio of gas i, and the function, $F_i(t)$, is a fitting function for the pure component i based on the Langmuir-Freundlich model:

$$n = \frac{a * b * p^{1/c}}{1 + b * p^{1/c}} + \frac{d * e * p^{1/f}}{1 + e * p^{1/f}}$$

In this equation, n is the gas uptake in mmol/g, p is the pressure in bar, and a, b, c, d, e, and f are the fitting parameters. Since $x_1 = 1 - x_2$ and $y_1 = 1 - y_2$, the integrated equation nets only three unknowns. Therefore, by specifying one value and varying a second, the third value can be calculated. Selectivity can then be calculated as:

$$s_{1,2} = \frac{x_1/y_1}{x_2/y_2}$$

Table S3. Langmuir-Freundlich fitting parameters and coefficient of determination for BLP-10(Cl).

Gas	Temp	a	b	c	d	e	f	R²
CO ₂	273 K	5.0698	0.4766	0.7407	1.5278	2.6425	1.0459	0.99999
	298 K	3.3663	0.2410	0.6351	1.3719	1.3214	0.9935	0.99999
CH ₄	273 K	3.6811	0.0570	1.0801				0.99979
N ₂	298 K	1.7589	0.1117	0.8398				0.99940

Figure S22: CO₂/CH₄ selectivity versus Pressure.

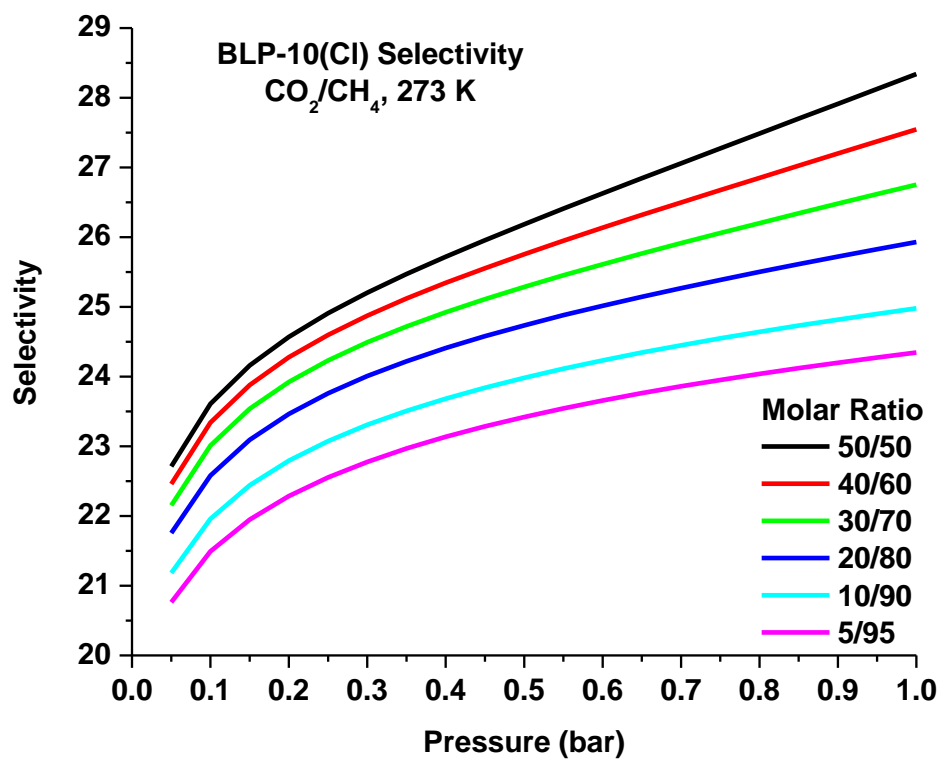


Figure S23: CO₂/CH₄ selectivity versus bulk phase molar ratio.

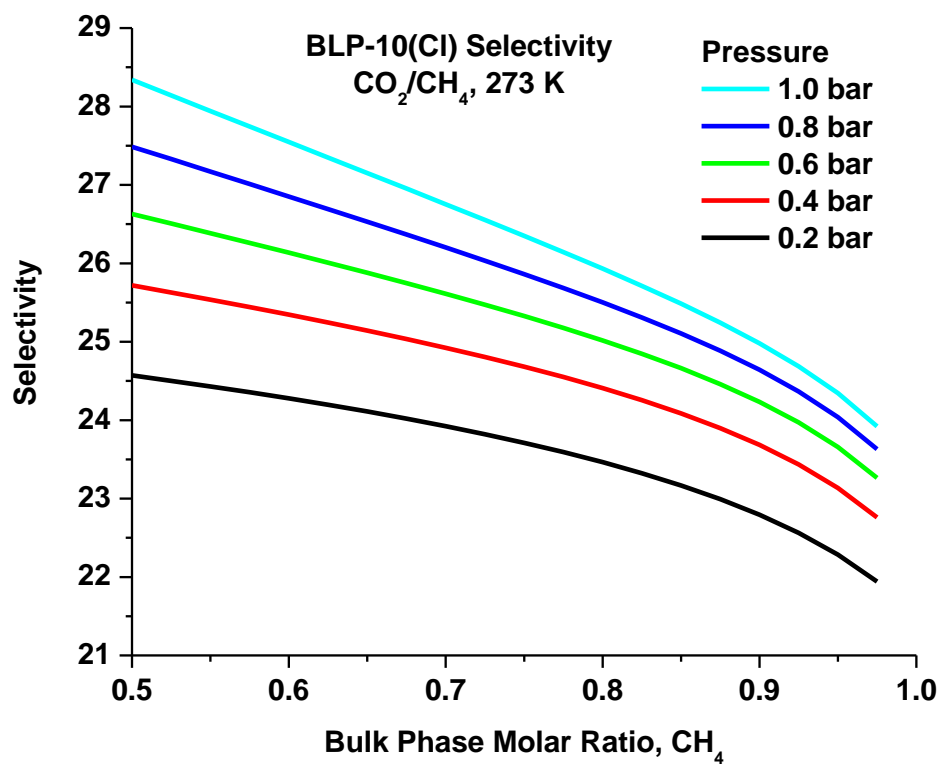


Figure S24: CO₂/N₂ selectivity versus Pressure.

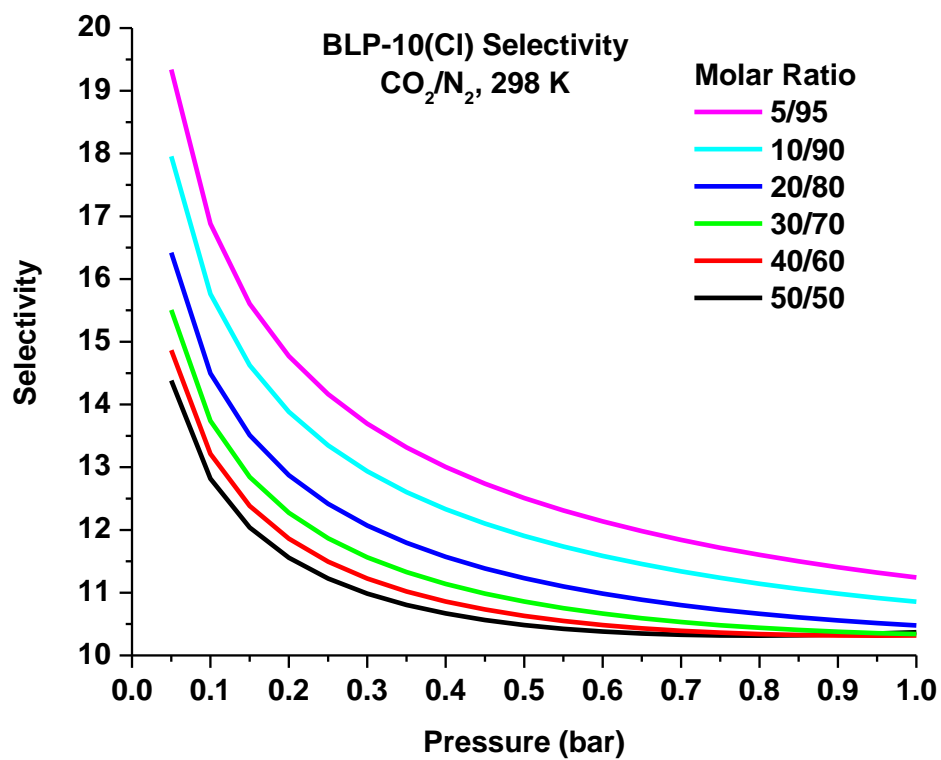


Figure S25: CO₂/N₂ selectivity versus bulk phase molar ratio.

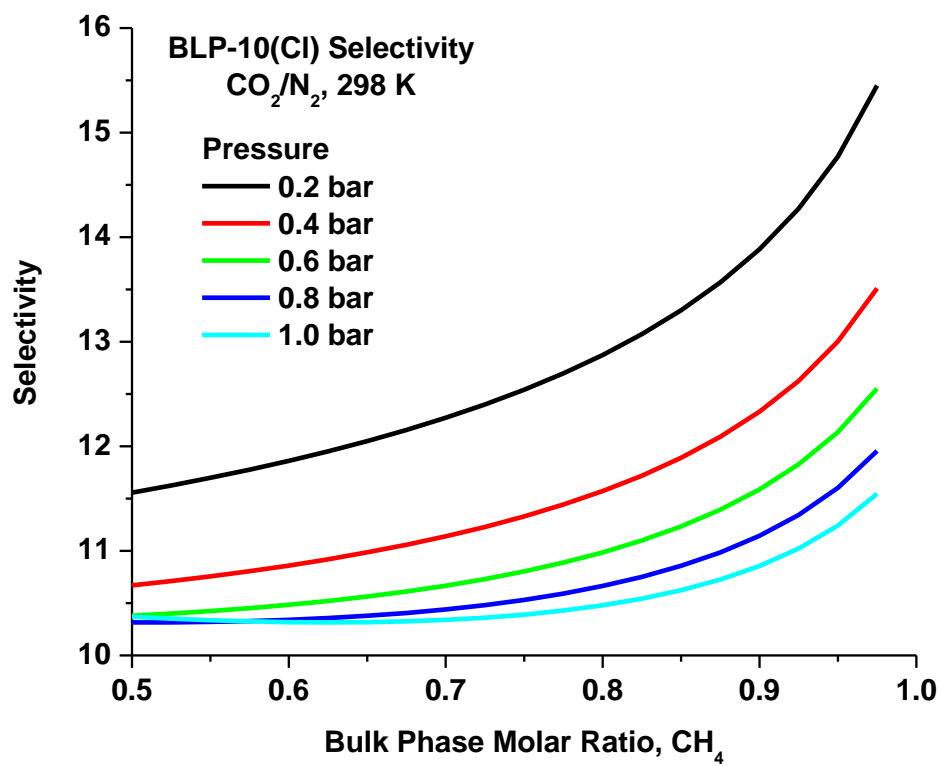
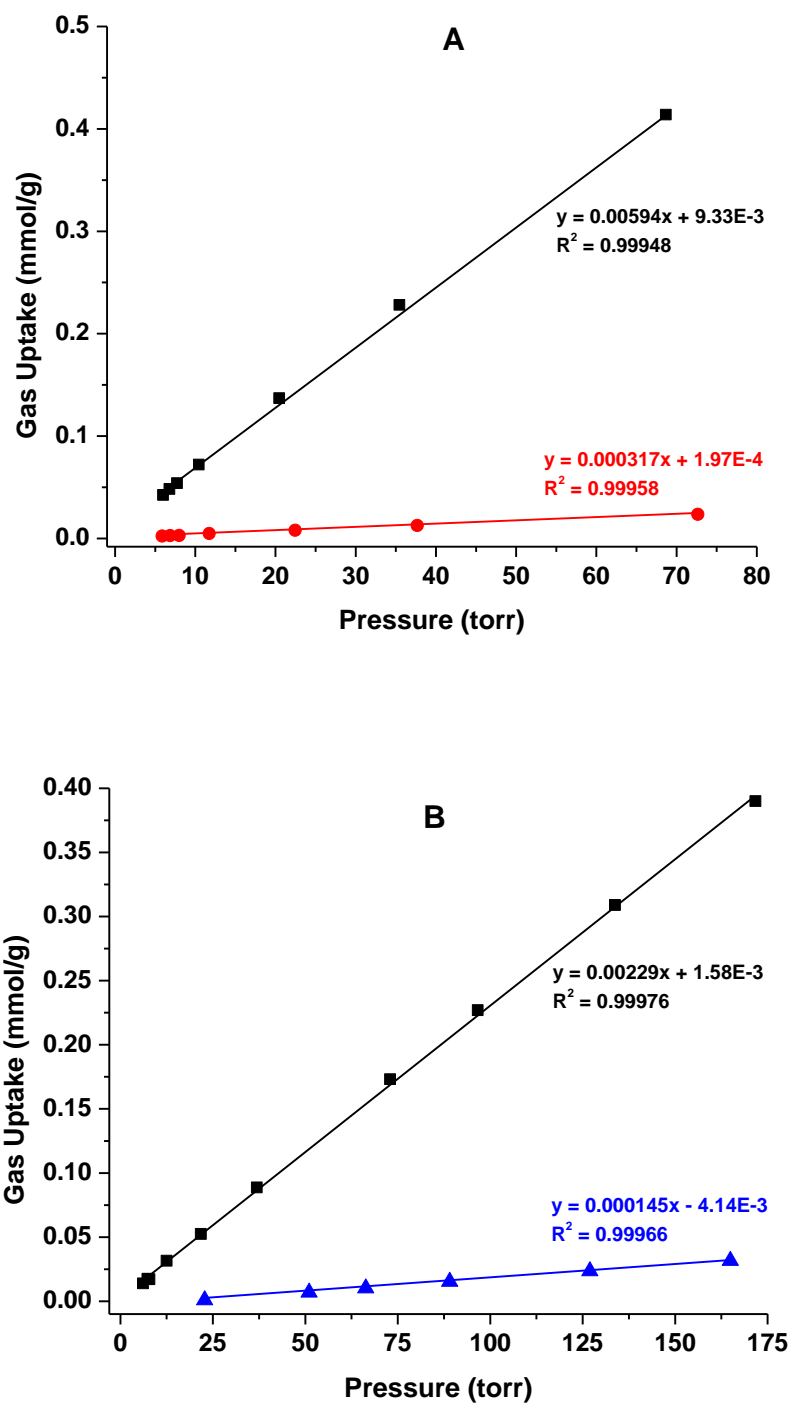


Figure S26: Adsorption Selectivity of CO₂ over CH₄ and N₂ for BLP-10(Cl) from initial slope calculations. CO₂ (black squares), CH₄ (red circles), and N₂ (blue triangles) isotherms collected at 273 K (A) and 298 K (B).



References

1. E. Lory and R. Porter, *J. Am. Chem. Soc.*, 1973, **95**, 1766.
2. H. Furukawa and O. M. Yaghi, *J. Am. Chem. Soc.*, 2009, **131**, 8875.
3. A. P. Cote, A. I. Benin, N. W. Ockwig, M. O’Keeffe, A. J. Matzger and O. M. Yaghi, *Science*, 2005, **310**, 1166.
4. A. D. Becke, *J. Chem. Phys.*, 1993, **98**, 5648.
5. S. H. Vosko, L. Wilk and M. Nusair, *Can. J. Phys.*, 1980, **58**, 1200.
6. Y. Zhao and D. G. Truhlar, *Theor. Chem. Acc.*, 2008, **120**, 215.
7. M. J. Frisch, G. N. Trucks, H. B. Schlegel et. al., Gaussian, Inc., Wallingford CT, 2009.
8. R. Krishnan, J. S. Binkley, R. Seeger and J. A. Pople, *J. Chem. Phys.*, 1980, **72**, 650.
9. A. D. McLean and G. S. Chandler, *J. Chem. Phys.*, 1980, **72**, 5639.
10. A. E. Reed, R. B. Weinstock and F. Weinhold, *J. Chem. Phys.*, 1985, **83**, 735.
11. A. L. Myers and J. M. Prausnitz, *AIChE J.*, 1965, **11**, 121.
12. Z. R. Herm, J. A. Swisher, B. Smit, R. Krishna and J. R. Long, *J. Am. Chem. Soc.*, 2011, **133**, 5664.